WALL PRESSURE STATISTICS IN A HIGH REYNOLDS NUMBER TURBULENT BOUNDARY LAYER

J.C. Klewicki, B.F. Perkins & M.M. Metzger
Physical Fluid Dynamics Laboratory
Department of Mechanical Engineering
University of Utah
Salt Lake City, Utah 84112, USA
klewicki@eng.utah.edu

ABSTRACT

In order to better understand boundary layer turbulence at high Reynolds number, the fluctuating wall pressure was measured within the turbulent boundary layer that forms over the salt playa of Utah's west desert. Pressure measurements simultaneously acquired from an array of nine microphones were analyzed and interpreted. The wall pressure intensity was computed and compared with low Reynolds number data. This analysis indicated that the variance in wall pressure increases logarithmically with Reynolds number. Computed autocorrelations provide evidence for a hierarchy of surface pressure producing scales. Space-time correlations are used to compute broadband advection velocities. The advection velocity data indicate an approximately logarithmic increase in U_a with increasing axial sensor separations. To the author's knowledge, the present pressure measurements, to date, constitute the highest Reynolds number, low noise, well resolved measurements of fluctuating surface pressure.

INTRODUCTION

The purpose of this paper is to explore the nature of wall pressure fluctuations beneath a high Reynolds number boundary layer. In this regard, the primary Reynolds number employed herein is based upon the boundary layer thickness, δ, and the friction velocity, $u_\tau = \sqrt{\tau_w/\rho}$, i.e., $\delta^+ = \delta u_\tau/\nu$, where ν is the kinematic viscosity. Efforts to reveal the detailed nature of high Reynolds number boundary layer turbulence encounter considerable technical challenges. Beyond those associated with actually generating a high δ^+ boundary layer, these challenges primarily relate to measuring the small scales and high frequencies of the turbulent motions characteristic of high speed laboratory flows, e.g., DeGraaff and Eaton (2000) and Metzger and Klewicki (2001). (Note that the most common way to achieve high Reynolds number in the laboratory is to operate at high speeds.) Regarding wall pressure, additional measurement challenges are associated with the non-negligible acoustic noise and facility vibration typical of even very high flow quality wind tunnels. These complications often require considerable data post-processing to extract reliable estimates of the true wall pressure signal, and even then the signal-to-noise ratios are generally not as high as desired. Thus, for example, even theoretically "well established" features of the wall pressure fluctuations, such as the k^{-1} spectral range, are often difficult to convincingly verify experimentally.

There is a firm theoretical foundation regarding the source of pressure fluctuations internal to the boundary layer, e.g., Blake (1986). Physically, these unsteady wall pressure signals arise from the weighted integral effect of the instantaneous motions internal to the turbulent boundary layer, e.g., Eckelmann (1990). Of course, knowledge and understanding of the nature and origin of these pressure sources is central to applications, for example, associated with attempts to reduce the acoustic signature radiated by submarines or high speed aircraft. As it pertains to the present effort, these two high Reynolds number applications are particularly relevant, since low noise wall pressure measurements that are also spatially and temporally resolved do not exist above moderate Reynolds numbers.

In this regard, existing high quality wind tunnel measurements are, to the author's knowledge, almost exclusively confined to Reynolds numbers less than about 1×10^4 (Farabee and Casarella 1991). Furthermore, only a subset of these measurements are able to report a normalized sensor diameter ($d^+ = du_\tau/\nu$) of less than about 90. The present results contribute to the understanding of boundary layer surface pressure by providing high Reynolds number ($\delta^+ \cong 1 \times 10^6$), high signal-to-noise ratio data, while maintaining very good spatial and temporal resolution.

EXPERIMENTAL CONSIDERATIONS

The following sections describe the unique facility employed, instrumentation configurations, as well as the procedures of the experiments and data analysis. An important aspect of this section is a documentation of the spatial and temporal resolution attributes of the microphone sensors employed.

SLTEST Facility

The present high Reynolds number experiments were conducted in the atmospheric surface layer that flows over the salt playa of Utah's west desert. As elucidated further below, the fluctuating wall pressure was measured within the turbulent boundary layer forming on the surface of the playa. The measurement site, the Surface Layer Turbulence and Environmental Science Test (SLTEST) facility, is located on the Dugway Proving Ground. Figure 2 shows an aerial depiction of the SLTEST site. As described in greater detail by Metzger and Klewicki (2001) and Klewicki and Metzger (2003), the SLTEST site is often characterized by consistent wind patterns and an extremely flat, homogenous terrain. The SLTEST facility also has permanent on-site power. Therefore, unlike

earlier studies performed at the site (Klewicki et al. 1995), these did not require portable generator-based power. This enabled the current microphone pressure measurements to be conducted within a environment almost entirely free from undesirable acoustic noise sources and, of course, completely devoid of any facility vibration.

The experimental measurements presented herein were acquired during field experiments in early June 2003. Relative to attaining the desired measurements, this early summer time frame is significant. That is, owing to the coupled effects of the naturally high water table and spring snow-melt, in the early summer the salt playa has a high moisture content that renders its maximal yearly smoothness while still being stable enough to support humans and equipment. During measurement periods in the early evening, flow often originates from the north ($>$ 150km fetch), and thus the flow is not disturbed by the surrounding hills to the east and west, see Fig. 2.

Experiment Description and Test Conditions

The bulk of the measurements presented were acquired on the evening of June 5, 2003. Relative to this, however, it is important to note that subsequent analyses of data acquired during same and subsequent years have yielded remarkably repeatable results, Kenney (2005). On the night of June 5, the flow came from the north with an average horizontal wind speed of about 4m/s at 2.5m above the surface.

As alluded to above, experiments performed later in the summer generally must contend with an increasingly rough surface owing to the drying and cracking caused by the intense summer heat. Since, however, the present experiments were conducted in the early part of the summer, the surface was much closer to hydraulically smooth – depending, of course, on the wind speed. In this regard, Fig. 1 shows a near-surface inner normalized mean velocity profile acquired during the same time at a location adjacent to the present surface pressure experiments, as well as previous measurement at the SLTEST site under $\simeq$smooth wall conditions. The relevant profile in Fig 1 is derived data simultaneously acquired from a vertical rake of hotwire sensors, sonic anemometers (CSI, model CSAT3) and minisodar (Aerovironment model 4000), Metzger (2005). As can be seen, the profile exhibits the expected $\sim$logarithmic variation with distance from the surface, as well as a downward shift associated with surface roughness. From this downward shift, the equivalent sand grain roughness was estimated at approximately 50 viscous units. The mean velocity measurements derived from the minisodar included in Fig. 1 indicate that the boundary layer thickness (top of the surface layer under near-neutral conditions) is about $\delta^+ = 1 \times 10^6$. This value is consistent with previous measurements at the SLTEST site, Metzger and Klewicki (2001), Priyadarshana and Klewicki (2004).

In order to best mimick the flow conditions of an isothermal wind tunnel, measurements were acquired prior to and continuing through sunset, which occurred at about 8:55pm. Through use of the Monin-Obukhov stability parameter, ζ, Fig. 3 characterizes the thermal stability conditions during each of the twelve $5-8$ minute data runs considered. The run durations are represented by the shaded regions on the figure. Sonic anemometer based measurements of $\zeta(t)$ were acquired at the heights of 2m, 3m, and 5m above the surface. As is clear, the surface layer transitions through a period of near neutral stability ($\zeta \approx 0$) near sunset. Previous measurements

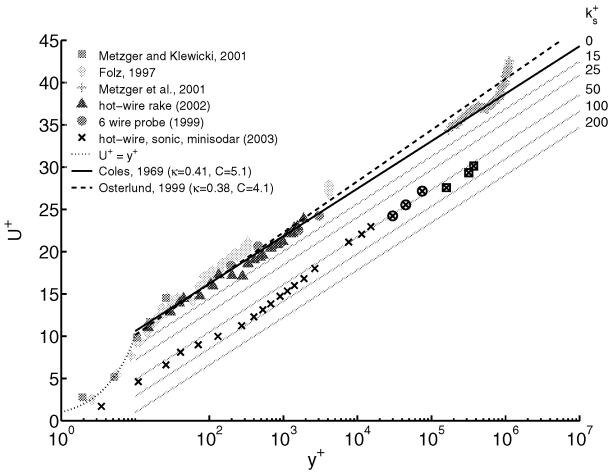

Figure 1: Inner normalized mean velocity profiles as derived from measurements simultaneously acquired from a vertical rake of hot-wire sensors, sonic anemometers and a minisodar, Metzger (2005).

indicate the thermal stability effects on turbulence structure are undetectable for a range of ζ near zero. Even more specifically, Metzger (2002) (also see, Klewicki and Metzger (2003)) has identified the time period near sunset during which ζ exhibits an approximately linear temporal dependence as the optimum time to acquire data containing the minimal effects of buoyancy. As can be seen from Fig. 3, for the night considered the time period over which ζ exhibits this behavior is particularly short. On the other hand, numerous microphone measurement comparisons (acquired both before and after the period of linear $\zeta(t)$) indicate that the surface pressure statistics and spectra are insensitive to small non-zero buoyancy effects. Under significantly unstable conditions, however, definite spectral features begin to appear. These results will be reported elsewhere.

For the present experiments, friction velocity ($u_\tau = \sqrt{\tau_w/\rho}$, where τ_w = wall shear stress) estimates as calculated from the 2m sonic amemometer Reynolds stress measurements were used to non-dimensionalize the data. Previous data reveal that under near-neutral conditions these estimates are within about 10% of those derived from floating element drag plate measurements, Metzger (2002). Thus, while sonic anemometer based estimates of u_τ are not of sufficient accuracy for resolving high sensisitivity questions, relating for example to the slope of the mean velocity profile, they are deemed sufficient for the less sensitive scaling issues addressed herein. In this regard, floating element drag plate measurements were also acquired during the present field experiments, and future normalizations of the present wall pressure data will utilize the u_τ values derived from these. In calculating an estimate for u_τ the kinematic viscosity ($\nu = 1.8 \times 10^{-5}$) was computed from the density, as derived from pressure and temperature data, and from the dynamic viscosity, as determined from the temperature.

Multi-sensor pressure measurements at axial and spanwise locations along the surface were acquired, analyzed, and interpreted. In connection with this, it is worth noting that two previous field trials using pressure transducers had been performed at the SLTEST facility. These studies utilized transducers having inherent low frequency cutoff frequencies

Figure 2: Aerial depiction of the Utah's west desert. ⊕ denotes the SLTEST facility location.

of 23Hz and 1.0Hz, (Klewicki et al., 2001, Klewicki and Miner 2002). The present flow is characterized by large length scales and low speeds, and owing to this, detection of the lowest frequencies using these sensors is shown below to be inadequate.

The current fluctuating surface pressure measurements were acquired from nine simultaneously operating microphones. The experimental configuration is depicted in Fig. 4. A set of hotwire probes mounted at the rear of the measurement plate were also employed to acquire axial velocity data simultaneously. Results from these sensors will be presented in a future paper. The wind vane situated atop the hotwire stand was used to visually align the array. This vane along with the circular rotatable plate allowed adjustment prior to acquiring data for each individual run.

As mentioned previously, the present flow is characterized by low speeds and large scales. Because of this, three different models of microphones were used to characterize the effects of their different low end cutoff frequencies relative to capturing the pressure spectrum. The microphones employed included two 0.25 inch Larson-Davis model 2250 microphones having a frequency response between 23Hz and 5kHz, three 0.5 inch Larson Davis model 900B microphones having a frequency response between 1.0Hz and 5kHz, and four 0.5 inch Bruel and Kjaer (model 4193L) microphones having a frequency response between 0.07Hz and 5kHz. To the author's knowledge, the latter of these capture the lowest frequencies of any commercially available microphone.

Table 1: Microphone Characteristics

Low Frequency cutoff	d(mm)
23Hz	6.35 (no cap)
1.0Hz	3.0 (pinhole)
0.07Hz	3.0 (pinhole)

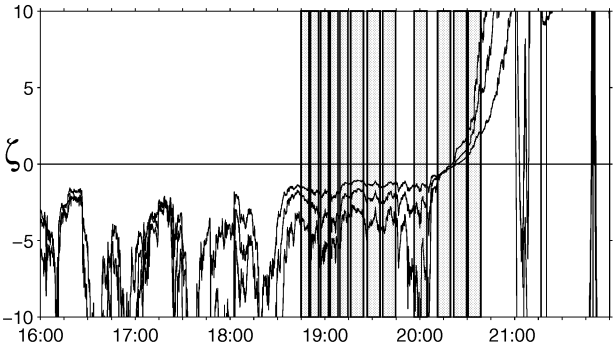

Figure 3: Temporal variation of the Monin-Obukhov stability parameter as computed from the vertical array of sonic anemometers. Background shaded regions denote the microphone array acquisition times. Measurements reported herein are from the data runs straddling $\zeta = 0$.

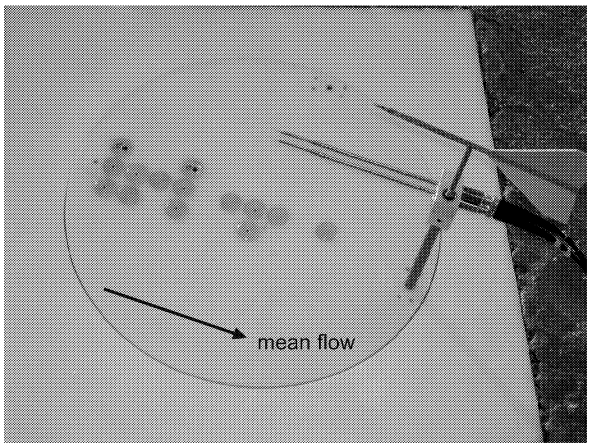

Figure 4: Experimental arrangement of the microphone array.

All of the 0.5 inch microphones were fitted with screw-on *pinhole* caps with 3mm diameter holes at the top. These, of course, where employed to reduce the effective sensing area of the microphones. Figure 5 shows a schematic of the pinhole caps. The caps were designed to have a Helmholtz resonator frequency exceeding 40kHz, as defined using Eq. 1, e.g., Kinsler and Frey (1950). In this equation, S is the cross sectional area of the opening, ℓ is the effective depth of the inlet hole, V is the volume of the cavity, and c is the speed of sound. This estimated resonator frequency is well outside the frequency range of the pressure fluctuations resident on the salt playa.

$$\omega_o = c\sqrt{\frac{S}{\ell V}} \tag{1}$$

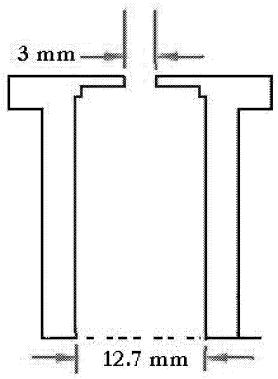

Figure 5: Microphone pinhole plug used to reduce the effective sensing area of the transducer.

Sensor Resolution and Signal Characteristics

All of the signals from the microphones were digitized at a sampling frequency of 5000Hz and stored on a laptop computer. The current experiments required no signal processing, aside from conversion of the voltage output from the transducers to Pascals through each transducer's respective calibration. As mentioned in the Introduction, this is very unusual since wall-pressure measurements generally re-

quire considerable post-processing to reduce extraneous noise associated with facility noise and vibration. This feature differentiates the present experiment from most wall pressure experiments conducted to date. The quality of the current data is illustrated by the computed pressure spectrum of Figure 6. Remarkably, this spectrum indicates over seven decades of signal amplitude above the noise floor, and for the 0.07Hz transducer about 3 decades of distinct f^{-1} variation.

Figure 6 also clearly reveals that the low frequency cut-off of the transducer strongly affects the capacity to measure the f^{-1} region of the spectrum. Based on estimates of the depth of the atmospheric surface layer, it is believed that the 0.07Hz transducers come very close to capturing the full spectrum of the wall pressure producing frequencies. The effect of low frequency cutoff relative to the capacity to capture the full spectrum is clearly shown in Figures 6 and 7. The starting points of the low end attenuation of these spectra corresponds closely to the respective microphone cutoff frequencies.

Figure 7 shows the anticipated decrease in pressure intensity as the low frequency cutoff of the transducer increases. The 0.07Hz transducer intensities are seen to be about 1.38 times greater than those derived from the 1.0Hz microphones. The data of Fig. 7 also reveal that when the 0.07Hz transducer signals are high pass filtered at 1.0Hz, they *identically* recover the results from the 1.0Hz transducers. This rather convincingly shows that the difference between the measured values of p'^+ from these two sensors is entirely resultant from their capacity to measure low frequencies. Additionally, since the 23Hz microphones did not utilize a pinhole cap, their $d^+(d^+{=}dU_\tau/\nu)$ values are considerably larger. However, by applying a 23Hz high pass filter to the 0.07Hz transducer data, and therefore mimicking the sensing capabilities of the 23Hz transducers at a smaller d^+ value, no deviation with increasing d^+ is observed. Thus, over the range of d^+ explored, the ability of the sensors to capture high frequency eddies appears essensentially independent of the transducer sensing diameter. Since none of the 0.07Hz transducers were used without a pinhole cap, the current experiment is unable to explore the sensitivity of capturing the low frequency contributions on d^+. On physical grounds, however, this effect is expected to be negligible.

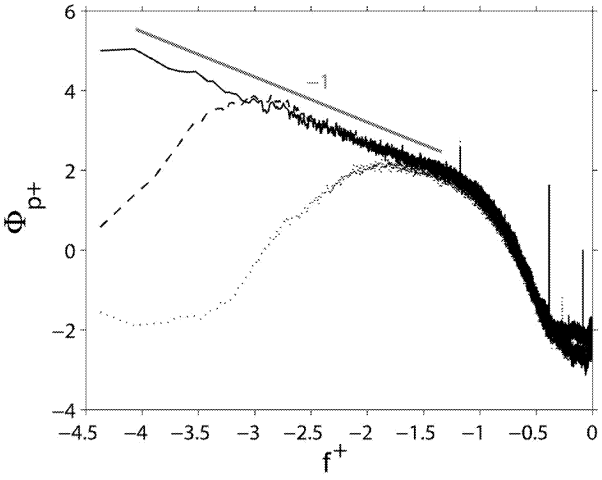

Figure 6: Inner normalized wall pressure spectra as derived from the different microphones.

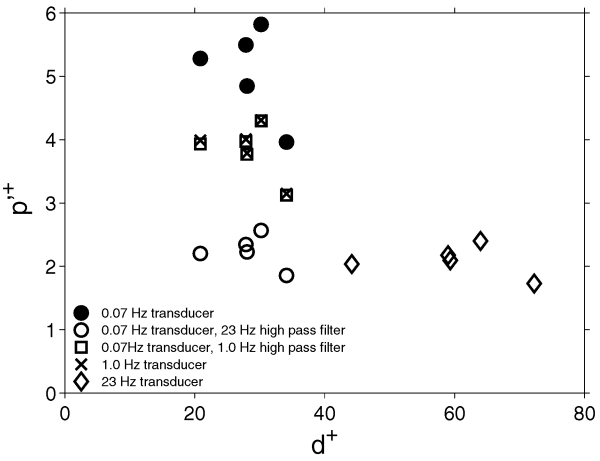

Figure 7: Inner normalized wall pressure intensities as a function of d^+ and high pass filter applied. Note that in all cases the frequency cited refers to the inherent low-pass cut-off frequency of the microphone.

RESULTS

The following sections explore the basic statistical and spectral structure of the fluctuating wall pressure measurements as derived from the present experiments. When appropriate, for the purposes of educing Reynolds number dependence, comparisons are made with low Reynolds number results.

Wall Pressure Intensities

Well-resolved wall pressure measurements at $\delta^+ = O(10^6)$ have not been previously reported. For this reason, it is useful to explore the Reynolds number dependence of the wall pressure intensity. Regarding this issue, Farabee and Casarella (1991) derive a semi-empirical formula for estimating p'^+ as a function of δ^+. The bases of this derivation are scaling arguments and empirical observations that the extent of the k^{-1} region of the wall pressure spectrum grows like the thickness of the logarithmic layer. Numerical integrations of estimated pressure spectra were then used to develop Eq. 2. This equation predicts a logarithmic dependence of the pressure intensity on Reynolds number, to within empircally determined constants. Figure 8 compares the present data point at $\delta^+ \approx 1 \times 10^6$ with data from previous low Reynolds number experiments. As can be seen, to within the error bars, the present data agree with the formula of Farabee and Casarella. Also depicted on Fig. 8 is a modified version of Eq. 2 (Eq. 3), with new empirical constants that more accurately capture the Reynolds number dependence indicated by the present data.

$$\frac{p_{rms}}{\tau_w} = \sqrt{6.5 + 1.86ln(\frac{R_\tau}{333})} \tag{2}$$

$$\frac{p_{rms}}{\tau_w} = \sqrt{6.5 + 2.30ln(\frac{R_\tau}{333})} \tag{3}$$

Space-time characteristics

Correlation data provide insights relating to the time-averaged spatial structure of the flow. This section examines autocorrelations and space-time correlations of the wall pres-

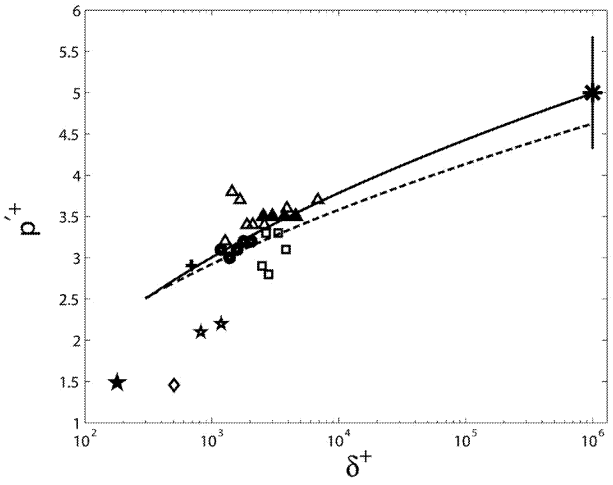

Figure 8: Inner normalized wall pressure intensities as a function of Reynolds number, δ^+. $*$: average of current data, error bar represents range of data scatter; ▲: Blake(1986), △: McGrath and Simpson (1987), □: Bull and Thomas (1976) (open pinhole), +: Schewe (1983), •: Farabee and Casarella (1991), ⋆: Horne (1989), ★: Choi and Moin (1990), ♢: Lauchle and Daniels (1987), – –, Eq. 2; –, Eq. 3.

sure. From the latter of these advection velocities of the pressure producing motions are estimated.

Autocorrelations of the wall-pressure as derived from the three different microphones are shown in Fig. 9. A primary feature of each of the curves is the negative peak at positive time delay. As indicated, however, the time delay to this negative peak is a strong function of the low frequency cutoff of the particular transducer. Remarkably, these results are interpreted to provide evidence of a distinguishable hierarchy of wall pressure producing scales present within the flow. In particular, the signals correlate longer (leading to the shift of the first zero crossing) when more of the large scale motions in the flow are captured by the microphones, i.e., the 23Hz low frequency cutoff transducer produces a signal that crosses zero at much shorter time delay than either the 1.0Hz and 0.07Hz low frequency cutoff transducers. That is, apparently self-similar regions of negative correlation are made evident depending on the low frequency cutoff of the microphone. This interpretation is further supported by the results found when the 0.07Hz transducers are high pass filtered at the frequencies of the other two transducers (not shown). In this case, the autocorrelation curves of the 1.0Hz and 23Hz transducers are closely replicated.

Figure 10 shows the time-delayed correlations between microphones separated by discreet Δx^+ increments. Broadband advection velocities may be estimated from such data. Specifically, the advection velocity of the surface pressure was calculated by determining the first peak in the correlation between pairs of transducers separated by some distance Δx^+. Advection velocities were then derived using the simple relation $U_a^+ = \Delta x^+/\delta t^+$. These are shown in Fig. 11 as a function of sensor separation. The normalized time-delays to the peak correlation for different streamwise sensor separations are depicted in Figure 10. Overall, the results of Fig. 11 reveal an increasing trend in U_a with increasing Δx^+. For the largest Δx^+ examined, $U_a^+ \approx 19$. A semi-logarithmic plot of the data in Fig. 11 (not shown) reveals that the observed increase in U_a^+ with Δx^+ is approximately logarithmic.

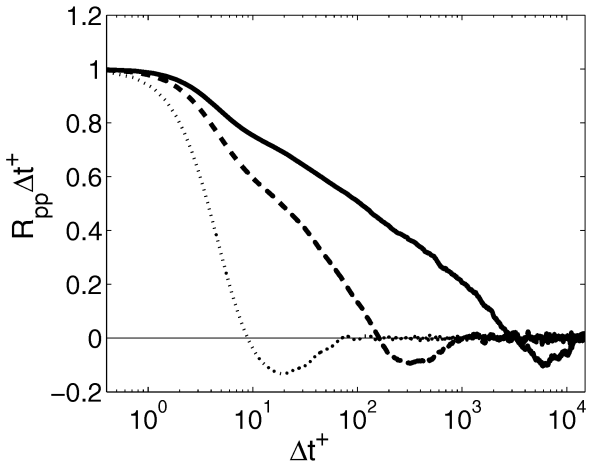

Figure 9: Autocorrelations of the surface pressure for the differing microphones; dotted line: 23Hz, dashed line: 1.0Hz, solid line: 0.07Hz.

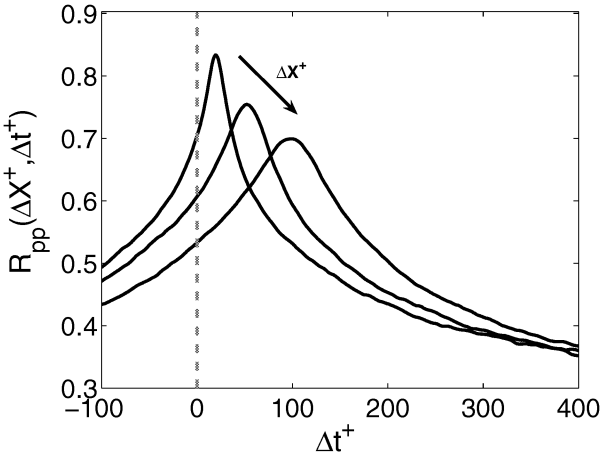

Figure 10: Temporal correlations of the surface press for varying Δx^+ as derived from the microphones having a 0.07Hz low frequency cut-off.

CONCLUSIONS

Spatially and temporally well-resolved measurements of the surface pressure were acquired beneath in the near-neutral atmospheric surface layer that flows over the salt playa of Utah's west desert. The measurements were acquired using microphones having three different low frequency cutoff values. Comparison of these measurements allowed important attributes relating to the spatial and temporal scales contained within the surface pressure to be discerned. To the author's knowledge, the present measurements constitute the highest δ^+, well-resolved pressure measurements to date.

From the present measurements the following are concluded.

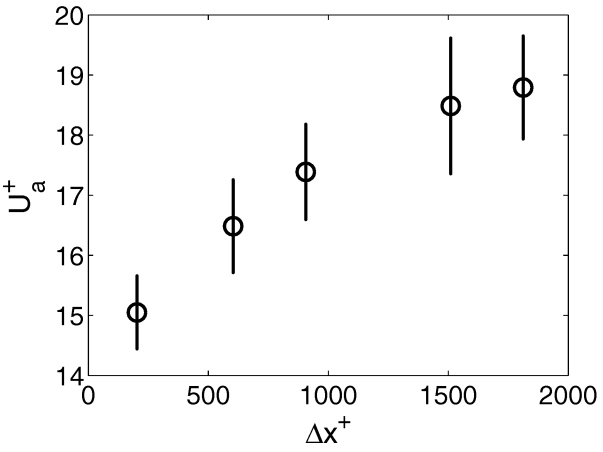

Figure 11: Broadband convection velocities computed as a function of Δx^+. Error bars indicate ± 1 standard deviation about the mean of the sample.

1. Increased low frequency attenuation was observed as the low-end cut-off frequency of the microphone increased. This indicates that the 1.0Hz and 23Hz transducers capture diminishing fractions of the total contribution to the surface pressure intensity. Based upon estimates of the surface layer thickness, the 0.07Hz microphones are believed to capture essentially all of the pressure fluctuations generated within the surface layer. Over the range of d^+ explored ($20 < d^+ < 75$), the ability of the sensors to capture the high frequency eddies is essentially independent of transducer sensing diameter.

2. A logarithmically increasing trend in the inner normalized wall pressure variance is observed for increasing δ^+. To within the scatter of the data, this trend is fit by the semi-theoretical result of Farabee and Casarella (1991). This previous result was modified to more accurately represent the variation of wall pressure intensity with increasing Reynolds number indicated herein. The present results extend the scaling of wall pressure by about 2.5 *decades* in δ^+.

3. An analysis of autocorrelations suggests that a distinct, self-similar, hierarchy of scales is inherently embedded within the wall pressure signal.

4. Broadband advection velocities, as derived from temporal correlations between spatially separated sensors, exhibit increasing values for increasing Δx^+ distances between the sensors. This increase is observed to be an approximately logarithmic function of Δx^+.

ACKNOWLEDGMENT

This work was supported by the National Science Foundation under grant CTS-0120061 (grant monitor, M. Plesniak) and the Office of Naval Research under grant N00014-00-1-0753 (grant monitor, R. Joslin).

REFERENCES

Blake, W. K., 1986. *Mechanics of Flow-Induced Sound and Vibration*, Academic Press, London.

Bull, M. K. and Thomas, A. S. 1976. "On the role of wall-pressure fluctuations in deterministic motions in the turbulent boundary layer", *J. Fluid Mech.*, Vol. 128, pp. 283-322.

Choi, H. and Moin, P. 1990. "On the space-time characteristics of wall pressure fluctuations", *Phys. Fluids A* Vol. 8, pp. 1450-1460.

DeGraaff, D. B. and Eaton, J. K. 2000. "Reynolds-number scaling of the flat-plate turbulent boundary layer", *J. Fluid Mech.*, Vol. 422, pp. 319-346.

Eckelmann H. 1990. "A review of knowledge on pressure fluctuations", Editors S.J. Kline and N.H. Afgan, *Near-Wall Turbulence: 1988 Zoran Zaric Memorial Conference*, Hemisphere Publishering Corp.: 328-347.

Farabee, T. M. and Casarella, M. J. 1991. "Spectral features of wall pressure fluctuations beneath turbulent boundary layers", *Phys. Fluids*, Vol. 3, pp. 2410-2420.

Horne, M. 1989. Ph.D. dissertation, The Catholic University of America, Washington, DC.

Kenney, D. 2005. "Surface Vorticity Flux Measurements in a High Reynolds Number Boundary Layer", M.S. Thesis, University of Utah, Salt Lake City, Utah.

Kinsler, L. E. and Frey, A. R. 1950. *Fundamentals of Acoustics*, 2nd Ed., John Wiley and Sons, Inc., New York, NY.

Klewicki J. C., Metzger, M. M. Kelner, E. and Thurlow, E. M. 1995. "Viscous sublayer flow visualizations at $R_\theta \simeq 1,500,000$", *Phys. Fluids*, Vol. 6, pp. 257-263.

Klewicki, J. C. and Metzger, M. M. 2003. "Studies of high Reynolds number turbulence in the atmospheric surface layer over the salt playa of western Utah", Editor A.J. Smits, *Reynolds Number Scaling in Turbulen Flow*, Kluwer Academic Publishers: 45-52.

Klewicki, J. C., Metzger, M. M., Perkins, B. F. and Priyadarshana, P. 2002. "Reynolds number effects on wall layer convection velocities", *AIAA paper no. 02-1109.*

Klewicki, J. C. and Miner, H. E. 2002. "Wall pressure structure at high Reynolds number", *American Physical Society, Division of Fluid Dynamics*, Dallas, TX, November 2002.

Lauchle, G. C. and Daniels, M. A. 1987. "Wall-pressure fluctuations in turbulent pipe flow" *Phys. Fluids*, Vol. 30, pp. 3019-3024.

McGrath, B. E. and Simpson, R. L. 1987. *NASA Contractor Report No. 4051.*

Metzger, M. M. and Klewicki, J. C. 2001. "A comparative study of wall region structure in high and low Reynolds number turbulent boundary layers", *Phys. Fluids*, Vol. 3, pp. 693-701.

Metzger, M. M. 2005. "Length and time scales of the near-surface axial velocity in a high Reynolds number turbulent boundary layer", proceedings of *Turbulent Shear Flows Phenomena 4*, Williamsburg, VA.

Panton, R. L. and Linebarger, J. H. 1974. "Wall pressure spectra calculations for equilibrium boundary layers", *J. Fluid Mech.*, Vol. 65, pp. 261-287.

Priyadarshana, P. and Klewicki, J. 2004. "Study of the motions contributing to the Reynolds stress in high and low Reynolds number turbulent boundary layers, *Phys. Fluids*, Vol. 16, pp. 4586-4600.